Photo-CIDNP studies on reaction centers of rhodobacter sphaeroides

Prakash, Shipra

6 Current view and Outlook

6.1 Introduction

Previous Chapters in this thesis have shown that experimental results in combination with theoretical explanations have been important for the understanding of photo-CIDNP. This Chapter starts with presenting the current view on all the mechanisms involved in photo-CIDNP. It then reports the first time-resolved experiments on the build-up of photo-CIDNP. These experiments form the basis for more detailed studies in the future. As a technique, photo-CIDNP could have numerous applications. The ideas for advances in this direction are presented in the last section of this Chapter.

In Chapter 2, the photo-CIDNP effect in bacterial reaction centers of *Rb. sphaeroides* WT has been described by contributions from two parallel mechanisms. First, the electron-electron-nuclear three spin mixing (TSM) involves the polarization transfer from the electron-electron zero-quantum transition to the nuclear spins (Jeschke, 1997, 1998). The TSM depends on the electron-electron coupling in the spin-correlated radical pair and the anisotropic hyperfine coupling. Second, in the Differential Decay (DD) mechanism the anisotropic hyperfine coupling can cause a net photo-CIDNP effect between the two electron spins even in the absence of coupling provided the spin-correlated radical pairs have different lifetimes in their singlet and triplet states (Polenova and McDermott, 1999). The field dependence of photo-CIDNP has been studied at three different magnetic field strengths for RCs of *Rb. sphaeroides*. The simulations of photo-CIDNP intensities for the WT presented in Chapter 2 are based on the TSM and DD mechanisms. In the simulations all signals are emissive (negative), which is in line with the WT experiments and the field dependence. The distribution of spin density over the donor molecules is reproduced remarkably well, which is encouraging. On the other hand, it is shown that for R26 a description in terms of TSM and DD is essentially incomplete, since an absorptive (positive) response is detected, which is tentatively attributed to an additional mechanism, Differential Relaxation (DR), involving the donor (Chapter 3).

In the past, the interpretation of MAS photo-CIDNP intensities has been restricted by incomplete understanding of the underlying mechanisms. By resolving the differences between R26 and WT and by providing a detailed comparison between data and theory, this thesis (*i*) arrives at a new and improved self-consistent picture of the transfer mechanisms, (*ii*) paves the way for future biophysical studies and (*iii*) guides the theory development into new, unexplored directions.

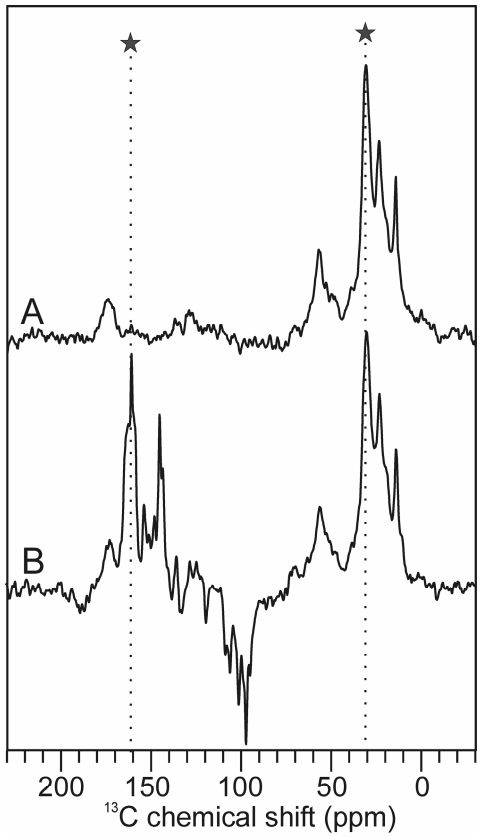

Figure 6.1. ^{13}C MAS NMR spectrum of *Rb. sphaeroides* R26 RC at 400 MHz, 223 K and a spinning frequency of 9 kHz in A) dark and B) under light. The peaks at 161 and 31 ppm used for determination of the build-up kinetics are marked with a star.

A sound experimental basis will ultimately lead to a consistent picture of the underlying mechanisms. In this respect, further theoretical developments will require extensive exploration of the anisotropy of the photo-CIDNP process as shown in Chapter 5 and time-resolved experiments to study the build-up of the polarization. The first steps in this direction are presented below.

6.2 The build-up of photo-CIDNP

The build-up to the steady state in photo-CIDNP takes ~500 photochemical cycles (see below). Studies of the build-up kinetics may help to quantify the contributions from the various mechanisms. The experimental kinetics of the photo-CIDNP build-up was thus studied by varying the light pulse length from 1 to 10 s.

Photo-CIDNP MAS NMR spectra were recorded from quinone-depleted RCs at 223 K and a field of 9.4 T using white light. The dark and photo-CIDNP spectra were recorded with a 90°-^{13}C pulse followed by a Hahn-echo and TPPM proton decoupling using a spinning frequency of 9 kHz. The build up was measured by placing a shutter in front of the fiber.

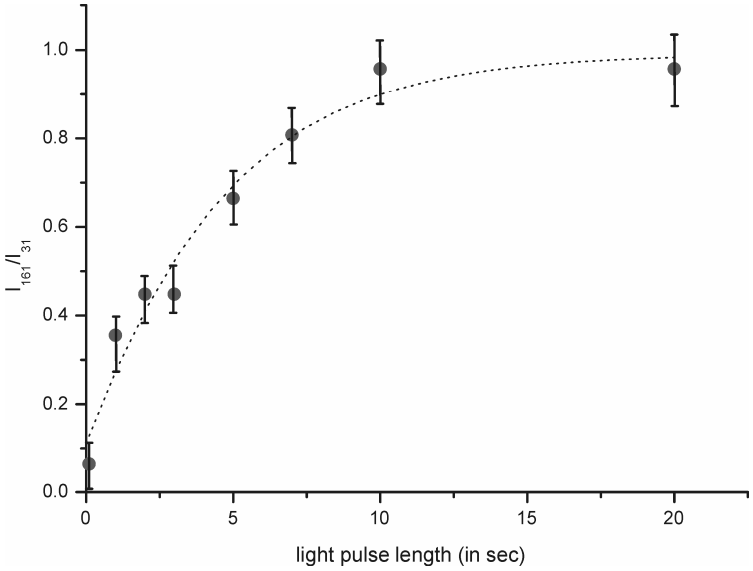

Figure 6.2. Build-up of light-induced nuclear polarization. The dashed line is the first order kinetics fit to the data.

The details of the light setup are described in Chapter 1. The light pulse was applied just before the 90º-^{13}C pulse. The delay between the light pulse and the 90º-^{13}C pulse was kept constant at 5 μs. The length of the light pulse plus 12 s was used always for relaxation as the recycle delay. 3k scans were collected for each experiment and a spinning frequency of 3.6 kHz was used.

6.2.1 Steady-state photo-CIDNP

Figure 6.1A shows the MAS NMR response from the protein matrix with strong signals in the aliphatic region and weak signals in the aromatic and carbonyl regions. The figure 6.1B has been obtained under continuous illumination with white light and represents photo-CIDNP in the steady state, i.e. a balance between light-induced production of nuclear polarisation on the one hand and relaxation on the other hand. Under these conditions, both enhanced absorptive (positive) and emissive (negative) signals are observed in the R26 RCs (Chapter 2 and 3). In natural abundance ^{13}C samples, spin diffusion can be neglected. All light-induced signals thus appear in the aromatic region and no enhancement is observed for signals in the aliphatic region. The emissive signals are detected in the region of methine carbon response. Thus, the signal in the aliphatic region (31 ppm), originating from the protein matrix, can be taken as an internal standard. In a similar way, the strongest light-induced signal at 161 ppm provides a standard for the photo-CIDNP intensity. Hence, both signals are good markers for studying the build-up of photo-CIDNP towards the steady state.

6.2.2 Build-up kinetics

Figure 6.2 shows the build-up of the light-induced nuclear polarization towards the steady state. Each point is the ratio of the intensities of the peak at 161 ppm to the peak at 31 ppm at

different light pulse lengths. A fit to first-order build-up kinetics I_{161}/I_{31} = 1- exp (-*kt*) +0.07 yields $k = 0.27\ s^{-1}$. The initial point (no light) is at 0.07 due to the background response from aromatic natural abundance ^{13}C in the dark spectrum. 50% of the steady-state photo-CIDNP is reached after ~ 4 s. After about ~ 10 s, the steady state is reached to ~ 90%. For comparable experimental conditions, an average value of 50 photons per second per RC has been estimated (Matysik et al., 2001a). Hence, the steady state is almost reached after ~500 photons per RC. The build-up kinetics of the absorptive and emissive signals is comparable. For the kinetics of the DD mechanism, the build-up of the steady state has been simulated by Polenova and McDermott (Polenova and McDermott, 1999), also assuming light excitation with 50 photons per second. Moreover, the time constant of $0.20\ s^{-1}$ for the simulated data is in line with $k = 0.27\ s^{-1}$ determined by the experimental data. The kinetic model proposed by Polenova and McDermott thus appears to be consistent with the data in figure 6.2. In fact, this is expected as the time scales of polarization build up from a single photon are less than 50 ns for the mechanisms are well separated from the build-up after more than 50 photons.

A mechanical shutter can not be extended to a nanosecond time resolution. This should be possible with a pulsed laser that produces nanosecond pulses. Such time-resolved studies with nanosecond time resolution would be ideal for probing the details of the single photon processes. In addition, time-resolved photo-CIDNP can be used to extract information on the electronic structure of the intermediate states of the photochemical cycle.

6.3 Ideas for application of photo-CIDNP

It has been shown that the photo-CIDNP MAS NMR intensities of the RCs of *Rb. sphaeroides* WT and R26 are enhanced by a factor of 10000 at a field strength of 4.7 T (Chapters 2 and 3). This strong enhancement in the photo-CIDNP MAS NMR intensities of the RCs can be used in many different ways for various applications. Some of these ideas are presented here.

6.3.1 Construction of artificial photosynthetic device

The first comprehensive map of the electronic ground state of the photochemically active cofactors in the RC has been presented in Chapter 4. In recent years, there has been a great deal of progress in mimicking the photosynthetic process by means of artificial molecular constructs based on porphyrins systems (Wasielewski, 1992). The knowledge about the electronic structure of the donor, P, the acceptor, Φ and the interaction with the histidine residue obtained from the bacterial RC provides sufficient impetus for strarting modelling studies with the aim of building artificial photosynthetic devices. Constructing models of such donor acceptor systems can be the first step in this direction. The model of the viable donor acceptor system can then be used to construct it through organic synthesis.

6.3.2 Use of photo-CIDNP as a 'spin torch'

Photo-CIDNP has been observed to diffuse away from the cofactors where it is generated (Matysik et al., 2001a; Matysik et al., 2001b). It can therefore be used as a 'spin torch'. This 'spin torch', based on a secondary polarization transfer mechanism such as spin diffusion, can explore the binding pocket in the reaction center and its influence on the cofactors. This may be done by labeling of particular amino acids in the binding pocket surrounding the cofactors in the active A-branch. The amino acids would gain polarization through spin diffusion from the cofactors and the polarization can then further diffuse to other parts of the protein backbone. 'Spin torches' may also be used to illuminate surfaces and to study the function of biological systems.

6.3.3 Study of intact cells with NMR

NMR is now routinely used to study structure, dynamics and functional mechanisms of biomacromolecules as well as for medical imaging. However, sensitivity and resolution are insufficient for routine investigations of molecules inside cells in the natural environment. On the other hand, the limited number of favorable cases where NMR of biomolecules in cells could be obtained have demonstrated the high potential of such studies. For instance, the metabolic composition in whole cells can be studied with High-Resolution Magic-Angle-Spinning (MAS) ^{1}H NMR provided a high concentration of cellular components is present (Chauton et al., 2003). Likewise, NMR images from single ova cells have been obtained but are limited to μm resolution (Aguayo et al., 1986). In this thesis it has been shown that the photo-CIDNP MAS NMR enabled the study of the special pair BChl molecules in the native cellular environment at nanomolar concentrations (Chapter 3). Photo-CIDNP MAS NMR can thus be extended to study cells from other photosynthetic bacteria.

6.3.4 Increasing sensitivity in Magnetic Resonance Imaging

Magnetic Resonance Imaging (MRI) as an experimental noninvasive technique can provide important information on physiological processes that is otherwise inaccessible. It can be used to study dynamic processes in biological systems. One such application is the investigation of the metabolic pathways in plants using ^{13}C labeled precursors (Köckenberger, 2001; Köckenberger et al., 2004). However, owing to the low sensitivity of ^{13}C NMR experiments, it is difficult to resolve ^{13}C tracers spatially in intact plants. In these experiments, if it is possible to transfer the primary polarization from the initially enhanced nuclei by photo-CIDNP to the secondary nuclei in plants, it might considerably increase the sensitivity. Contrast agents are added for better images of MRI, but these contrast agents are not always generally applicable. In this instance, 'spin torches' could provide a very good alternative.

6.3.5 Detection of a single nuclear spin with photo-CIDNP MRFM

Magnetic Resonance Force Microscopy (MRFM) in combination with photo-CIDNP may provide a method to overcome the inherent insensitivity of NMR allowing the detection of a single spin. Recently, a single electron spin has been detected by MRFM (Rugar et al., 2004). MRFM is based on mechanical detection using an AFM-type cantilever. The principle is based on the fact that when a sample carrying a magnetic dipole moment is put on a cantilever, a force $F_z = M_z \cdot \partial B/\partial z$ is exerted on this lever in the presence of a magnetic field gradient (Verhagen, 2002). The magnetization and, therefore, the force is made time dependent by inverting the magnetization adiabatically. This process then matches the cantilever frequency resulting in a oscillatory deflection observed in the MRFM experiment. MRFM has been used to observe quadropolar nuclei in ^{69}Ga, ^{71}Ga and ^{27}Al in device-type GaAs and AlGaAs layers (Verhagen et al., 2002). On the other hand, cofactors in intact cells have been observed at atomic resolution with photo-CIDNP (Chapter 3). MRFM in combination with photo-CIDNP may be used for looking at single nuclear spins in the cofactor molecules inside a cell.

To conclude, the great improvement in NMR signal sensitivity and selectivity reached with this thesis provides a number of applications in the world of magnetic resonance techniques. Hence, the author expects that photo-CIDNP will play an important role in the current efforts to overcome the intrinsic limits of NMR.